What is the longitudinal magneto-optical Kerr effect?

Jon Ander Arregi[1], Patricia Riego[1,2], and Andreas Berger[1]

[1]*CIC nanoGUNE, Tolosa Hiribidea 76, E-20018 Donostia–San Sebastián, Spain*

[2]*Departamento de Física de la Materia Condensada, Universidad del País Vasco, UPV/EHU, E-48080 Bilbao, Spain*

*E-mail: j.arregi@nanogune.eu

Abstract

We explore the commonly used classification scheme for the magneto-optical Kerr effect (MOKE), which essentially utilizes a dual definition based simultaneously on the Cartesian coordinate components of the magnetization vector with respect to the plane of incidence reference frame **and** specific elements of the reflection matrix, which describes light reflection from a ferromagnetic surface. We find that an unambiguous correspondence in between reflection matrix elements and magnetization components is valid only in special cases, while in more general cases, it leads to inconsistencies due to an intermixing of the presumed separate effects of longitudinal, transverse and polar MOKE. As an example, we investigate in this work both theoretically and experimentally a material that possesses anisotropic magneto-optical properties in accordance with its crystal symmetry. The derived equations, which specifically predict a so-far unknown polarization effect for the transverse magnetization component, are confirmed by detailed experiments on epitaxial hcp Co films. The results indicate that magneto-optical anisotropy causes significant deviations from the commonly employed MOKE data interpretation. Our work addresses the associated anomalies, provides a suitable analysis route for reliable MOKE magnetometry procedures, and proposes a revised MOKE terminology scheme.

1

Over the last decades, the magneto-optical Kerr effect (MOKE) has gained widespread popularity as a characterization tool for the study of magnetism and magnetic materials [1,2]. MOKE proved to be especially well suited to investigate magnetization effects at the nanoscale where it was first utilized in 1985 by Moog and Bader to measure magnetic hysteresis loops of Fe monolayer films [3]. Nowadays it constitutes a widely employed form of magnetometry with the ability to obtain vector [4-8] and depth- or layer-resolved magnetization information [9-11]. Apart from enabling domain imaging when combined with light microscopy [12], it has also been successfully employed for the analysis of single nanostructures [13-15] and periodic magnetic lattices, by making use of the diffracted light signals [16]. Furthermore, MOKE constitutes the only viable method, by which magnetization dynamics can be studied down to the femtosecond time scale, namely via ultrafast laser pulses [17-19], and it is crucially important in emerging fields with significant technological potential such as all-optical switching [20,21] and magnetoplasmonics [22].

In any MOKE study, the experimentally accessible quantities are related to the Fresnel coefficients, which describe light reflection and are specifically defined as the complex ratios between the reflected (*r*) and the incident (*i*) electric field amplitudes $r_{mn} = E_{r,m}/E_{i,n}$. Here, the indices *m*, *n* stand for the orthogonal *s*- or *p*-polarization components of light [see Fig. 1(a)]. Assuming first-order magneto-optical Kerr effects and defining the plane of incidence as the *xz* plane of the laboratory frame, the magnetization dependent Fresnel coefficients are given in the literature as [1,2]

$$R = \begin{pmatrix} r_{ss} & r_{sp} \\ r_{ps} & r_{pp} \end{pmatrix} = \begin{pmatrix} r_s & \alpha m_x + \gamma m_z \\ -\alpha m_x + \gamma m_z & r_p + \beta m_y \end{pmatrix}$$

$$(1),$$

with α, β and γ being complex numbers, while m_x, m_y and m_z are the normalized magnetization components in Cartesian coordinates. The relative orientation of the plane of incidence, the magnetization components and the laboratory frame is indicated in Fig. 1. One can readily conclude from Eq. (1) that each orthogonal magnetization component has an unambiguous effect onto the polarization dependent reflectivity changes. In particular,

components m_x and m_z, which are contained in the plane of incidence, produce an intermixing of the s- and p-polarization, such that the reflected wave generally acquires a magnetization dependent rotation of the polarization axis θ_K and an ellipticity ε_K. On the other hand, m_y only generates a change in the r_{pp} reflectivity. This specificity to each magnetization component now motivates the nomenclature that is being used in literature for the different Kerr geometries, which are the well-known longitudinal, transverse and polar Kerr effects for the m_x, m_y and m_z components of the magnetization vector, respectively [1]. ==Furthermore, this specificity also constitutes the key characteristic, by which the behavior of individual magnetization components can be extracted from a MOKE experiment. Apart from sharing distinct symmetry properties with respect to incident and reflected polarization states, it is also commonly found that the polar Kerr effect, originating from m_z, is significantly larger than the longitudinal or transverse Kerr effects [21].== However, one has to keep in mind that the derivation of Eq. (1) is generally being accomplished by using a particular choice for the dielectric tensor of the magnetic material, namely [1,2]

$$\overset{\leftrightarrow}{\boldsymbol{\varepsilon}} = (\varepsilon_{ij}) = N^2 \begin{pmatrix} 1 & iQm_z & -iQm_y \\ -iQm_z & 1 & iQm_x \\ iQm_y & -iQm_x & 1 \end{pmatrix}$$

$$(2),$$

where the complex quantities N and Q are the refractive index and magneto-optical coupling factor of the material, respectively [footnote#1]. Specifically, the dielectric tensor in Eq. (2) describes a material, in which the magneto-optical coupling factor Q is the same irrespective of the magnetization orientation. Here, we label this situation as *magneto-optical isotropy*.

In this Letter, we explore the general validity of Eq. (1) and the associated MOKE classification scheme based upon orthogonal magnetization components. We find that in a more general case, Eq. (1) is actually not valid and thus a revised MOKE terminology has to be considered. For this purpose, we investigate both theoretically and experimentally a material that possesses anisotropic magneto-optical properties, such that Q acquires different values for different magnetization orientations, hereby reflecting the crystal symmetry. The derived

equations are confirmed by detailed experiments on epitaxial hcp Co films. Our results indicate that magneto-optical anisotropy causes significant deviations from the widely employed MOKE methodology and classification scheme. Our work addresses these associated anomalies, provides a suitable analysis route for reliable MOKE magnetometry procedures, and reflects the need for a more precise MOKE terminology scheme.

Without limiting the generality of our investigation, we focus in the following on the MOKE polarization effects associated with r_{sp}/r_p [footnote#2]. This effect is usually described in terms of a rotation θ_K and an ellipticity ε_K acquired upon reflection. By considering a bulk-like medium that is magnetized in the plane of the air/medium interface ($m_z = 0$), the Kerr rotation and ellipticity in the magneto-optically isotropic case is given by [1,2,23]

$$\theta_K + i\varepsilon_K = \frac{r_{sp}}{r_p} = \tilde{\alpha} m_x$$

(3),

with $\tilde{\alpha} = -iNQ \cos\theta \tan\theta' / [(N\cos\theta - \cos\theta')(\cos\theta + N\cos\theta')]$ being dependent on N, Q, as well as the incident and refraction angles θ and θ'. Thus θ_K and ε_K are proportional to m_x, and it is for this reason that the ratio r_{sp}/r_p is commonly termed as the *longitudinal magneto-optical Kerr effect*, since it entails the polarization state modification of light as a result of a *longitudinal magnetization* only. However, we will see that this is a special case, which results from the assumption of magneto-optical isotropy in Eq. (2).

We now consider a more general dielectric tensor than in Eq. (2). For crystals with uniaxial symmetry, two different magneto-optical coupling factors can occur, namely $Q_\parallel$ and $Q_\perp$, for magnetizations along and perpendicular to the symmetry axis (c-axis), respectively, so that in the absence of optical anisotropy, we have

$$\overleftrightarrow{\varepsilon} = (\varepsilon_{ij}) = N^2 \begin{pmatrix} 1 & iQ_\perp m_z & -iQ_\perp m_y \\ -iQ_\perp m_z & 1 & iQ_\parallel m_x \\ iQ_\perp m_y & -iQ_\parallel m_x & 1 \end{pmatrix}$$

(4)

for the specific case in which the c-axis is oriented along the x-axis [25]. To describe a more general case yet, we conduct an arbitrary rotation of the crystalline c-axis in the xy plane, which is given by the air/material interface. In order to do so, one has to transform the dielectric tensor in Eq. (4) accordingly, such that $\overleftrightarrow{\varepsilon}'(\Phi_0, \boldsymbol{m}) = \mathcal{R}(\Phi_0) \cdot \overleftrightarrow{\varepsilon}(\boldsymbol{m}) \cdot \mathcal{R}^T(\Phi_0)$, with $\mathcal{R}(\Phi_0)$ being the matrix corresponding to a rotation transformation by an angle Φ_0 about the z-axis. After performing this rotation operation, it turns out that the only dielectric tensor elements that are modified with respect to Eq. (4) are [26]

$$\varepsilon'_{13} = -\varepsilon'_{31} = -iN^2 Q_\parallel \left[(1 + \tau \cos^2 \Phi_0)m_y - \tau \cos \Phi_0 \sin \Phi_0 \, m_x\right]$$

$$\varepsilon'_{23} = -\varepsilon'_{32} = iN^2 Q_\parallel \left[(1 + \tau \sin^2 \Phi_0)m_x - \tau \cos \Phi_0 \sin \Phi_0 \, m_y\right]$$

$$(5),$$

for which we have utilized the magneto-optical anisotropy coefficient $\tau = (Q_\perp - Q_\parallel)/Q_\parallel$. From Eq. (5), we see that these particular off-diagonal tensor elements most generally depend on both in-plane magnetization components m_x and m_y instead of only one each. Under the assumption that $m_z = 0$, the corresponding Kerr rotation and ellipticity for incoming p-polarized light are now given as

$$\theta_K + i\varepsilon_K = \tilde{\alpha}' \left[(1 + \tau \sin^2 \Phi_0) \, m_x - \tau \cos \Phi_0 \sin \Phi_0 \, m_y\right]$$

$$(6),$$

where we have introduced the modified prefactor $\tilde{\alpha}' = -iNQ_\parallel \cos\theta \tan\theta' / [(N \cos\theta - \cos\theta')(\cos\theta + N \cos\theta')]$. It is clear from Eq. (6) that if $Q_\parallel = Q_\perp$ (i.e., $\tau = 0$), we recover Eq. (3). In the same manner, the dependence of θ_K and ε_K on m_x only is restored for Φ_0 values that align the c-axis with either the x- or y-axis, that is, for $\Phi_0 = 0°, \pm90°, \pm180°$. The inset in Fig. 1(b) contains the definition of the relevant axes and angles here.

Thus Eq. (6) reveals that, under the presence of anisotropic magneto-optics, a transverse magnetization component m_y contributes to the r_{sp}/r_p ratio, inducing a nonzero Kerr rotation and ellipticity. This situation is illustrated in Fig. 1, where a MOKE experiment under the presence of incoming p-polarized light and a transverse magnetization component alone is

5

sketched. Under isotropic magneto-optics conditions [Fig. 1(a)] the reflection of light gives rise to a change in reflectivity, while maintaining a p-polarized state for the outgoing beam. On the other hand, any level of Q anisotropy ($\tau \neq 0$) and any misalignment of the symmetry axis with respect to the plane of incidence cause the reflected wave to acquire an actual Kerr rotation and ellipticity [Fig. 1(b)]. This constitutes a strongly counter-intuitive concept within the context of conventionally defined MOKE magnetometry, as it contradicts the widely accepted notion that m_x can be directly inferred from the measurement of θ_K or ε_K, which is based on the idea, only valid in the magneto-optical isotropy case, that the m_y component contributes to changes in the r_{pp} reflectivity alone [26].

In order to experimentally verify the conclusions derived above, we conceived an experiment that is based upon the variation of magneto-optical anisotropy in epitaxial hcp Co films through interface modifications. In an early work on magneto-optical anisotropy, Weller *et al.* showed that in contrast to fcc Co, which exhibits crystallographic orientation independent magneto-optical properties, hcp Co possesses a pair of dissimilar magneto-optical coupling strengths $Q_\parallel$ and $Q_\perp$, for magnetization orientations that are parallel or perpendicular to the c-axis, respectively [27]. While this anisotropy in Q was initially quantified to be around 10% for photon energies near 2 eV [28], we recently found that this anisotropy amplitude can be greatly altered by modifying the strain state of hcp Co films [29]. However, we also observed that such a strain modification causes at the same time a variation of the magnetocrystalline anisotropy, making it impossible to influence magneto-optical anisotropy independently from magnetic anisotropy. With the aim of producing Co films with different amplitude of magneto-optical anisotropy but identical magnetic properties (e.g., magnetic anisotropy) we followed the strategy of growing a wedge-type overcoat of varying Ru-thickness onto the same Co film. This idea is based on the observation that a modification of magneto-optical anisotropy and the overall size of the magneto-optical effect can occur upon capping Co films with ultrathin metal layers that facilitate an increased spin-orbit coupling such as Ru [30, 31]. Another crucial aspect for our study here is the fact that hcp Co films with in-plane c-axis geometry exhibit a very

simple magnetization reversal behavior, which is dominated by magnetization rotation and switching, and produces uniform magnetization states for nearly all external field strengths and orientations [29,30,32,33]. Thus, we fabricated 20 nm thick hcp Co films with in-plane c-axis orientation via sputter deposition onto hydrofluoric acid etched silicon substrates of an elongated shape, 80 mm × 5 mm in size. We employed the epitaxial sequence Si(110)/Ag(110)/Cr(211)/Co(10$\underline{1}$0), for which we deposited 75 nm of Ag and 40 nm of Cr as template layers [32,33]. The deposition up to this step was carried out by rotating the substrate holder in order to obtain good film thickness uniformity. In the subsequent growth step, the substrate was aligned with its long axis towards the direction of a tilted sputter gun, so that a position dependent Ru-thickness could be obtained. Fig. 2(a) shows a schematic of the fabricated sample, with the thickness profile of the Ru-wedge being displayed in Fig 2(b), which was calibrated by spectroscopic ellipsometry (SE) and confirmed by x-ray reflectivity (XRR). We also tested the crystalline quality of the film stack by multiple x-ray diffraction measurements along the wedge, confirming its good epitaxy, similar to the quality that we reported previously [29,33].

For the present study, two 5 mm long segments named Sample A and B were cut from the fabricated sample, having Ru thicknesses of 0.3 and 1.6 nm, respectively. These segments are indicated as the shaded areas in Fig. 2(b). For the purpose of verifying that the two samples are magnetically equivalent, we characterized them via an independent technique. Specifically, we used a *MicroMagTM 3900* vibrating sample magnetometer (VSM), equipped with a 360° rotational stage that allows measurements for different azimuthal orientations of the sample. With this system, we acquired room temperature hysteresis loops for various orientations Φ_0 of the c-axis with respect to an in-plane oriented magnetic field, which was applied along the x-axis. Thus, we measured the field projected magnetization component $m = M/M_S = \cos\varphi$, with φ being the deviation of magnetization from the x-axis [see the inset in Fig. 1(b)]. The results for Sample A and B are depicted in Figs. 2(c) and 2(d) as color-coded magnetization maps vs. applied field strength H and c-axis orientation Φ_0. The data reveal that both samples

show a marked uniaxial magnetic anisotropy with the c-axis of Co being the preferential axis of magnetization. Moreover, the subtraction of the maps in Figs. 2(c) and 2(d), which is displayed in Fig. 2(e), shows a nearly perfect null signal and thus indicates that the m vs. H behavior is nearly identical in both samples. In order to obtain a quantitative estimate of the magnetic equivalence of both samples, we have performed least-squares fits of the VSM data to the energy expression $E = K_1 \sin^2(\varphi - \Phi_0) + K_2 \sin^4(\varphi - \Phi_0) - H M_S \cos\varphi$. From here, we have extracted the magnetic anisotropy fields $H_{K1} = 2K_1/M_S$ and $H_{K2} = 4K_2/M_S$ as well as the saturation magnetization M_S as fit parameters for both samples. The fitted parameters, contained in the top part of Table 1, indicate that the saturation magnetization values of the two samples under study are equal within the error bars, while the anisotropy fields H_{K1} and H_{K2} are only marginally different. This confirms that the ultrathin metal overcoat does not influence the saturation magnetization of our 20 nm thick magnetic films and modifies its magnetic anisotropy characteristics only minimally. As a matter of fact, we measured the variation of magnetic anisotropy for a set of Ru overcoat thicknesses along the wedge and found no noticeable trend. Altogether, this confirms that Sample A and B are magnetically equivalent, hence displaying equal $m(H)$ magnetization reversal paths [footnote#3]. Therefore, our VSM measurements allowed for an independent confirmation of the nominally identical magnetic behavior of both samples having different Ru-thickness overcoats, which is an important reference for our investigation of their magneto-optical properties. Using MOKE measurements, we verified their exact level of magneto-optical anisotropy by extracting $Q_\parallel$ and $Q_\perp$ [26], and we found that samples A and B show a substantially different value of τ, hence validating our fabrication strategy. The results for magneto-optical properties are summarized in the bottom part of Table 1.

For our MOKE measurements, we utilized an experimental setup with a laser light source ($\lambda = 635$ nm) that illuminates the sample at a 45° angle of incidence. The sample was mounted on a rotating stage to enable the variation of the angle Φ_0 in between the c-axis and x-axis, along which we applied a magnetic field by means of an electromagnet. For the

polarization analysis, we employed the generalized magneto-optical ellipsometry (GME) technique, by which the entire reflection matrix can be determined with a high degree of precision [5,6,29,30,34,35]. From the GME data, we extracted θ_K and ε_K as a function of H for incoming p-polarized light, for different sample orientations Φ_0. GME has the advantage that its detection scheme removes quadratic magneto-optical effects from the analysis [5,29,35], which is especially relevant here given that higher-order Kerr effects are commonly anisotropic [36]. Fig. 3 shows the measured θ_K (left panel) and ε_K (right panel) values for the decreasing field branch for samples A and B. We chose values of Φ_0 that orient the c-axis of Co nearly perpendicular to the applied field orientation, in order to achieve a substantial level of magnetization rotation, and thus cover a wide range of different magnetization orientations in the experiment. Figs. 3(a) and 3(b) display Kerr rotation and ellipticity values for $\Phi_0 = -90°$, which corresponds to the hard axis loop case. The θ_K and ε_K data for Sample A and B lie on top of each other, which highlights the identical reversal pathway of the samples. However, a slight difference in between the datasets for the two samples is already observed in Figs. 3(c) and 3(d), corresponding to the $\Phi_0 = -88°$ sample orientation, despite the fact that both samples undergo identical $m(H)$ magnetization rotation paths. This difference becomes increasingly larger for the sample orientations $\Phi_0 = -86°$ and $-84°$, as shown in Figs. 3(e)-(f) and 3(g)-(h). We attribute this behavior to magneto-optical anisotropy, which erases the field dependence equivalency between θ_K, ε_K and the longitudinal magnetization component, as anticipated in Eq. (6). As can be observed in Fig. 3, the field values at which each θ_K or ε_K become equal to zero are consistently larger for Sample B than for Sample A. This difference increases monotonically as Φ_0 shifts away from $-90°$. To visualize this better, the Φ_0 dependence of the difference in zero-crossing fields $\Delta H_0 = H_0^B - H_0^A$ is shown in Fig. 4 as extracted from the θ_K and ε_K data sets, and compared to values obtained from magnetization measurements via VSM. It can be seen that VSM measured ΔH_0 data exhibit near zero values for all Φ_0. Contrary to this purely magnetic results, ΔH_0 values retrieved from our MOKE data exhibit a very substantial

and nearly linear increase with Φ_0, reaching values of more than 100 Oe and 300 Oe at $\Phi_0 = -84°$ for measurements based upon the Kerr ellipticity ε_K and rotation θ_K, respectively.

One can understand the differences in between the samples shown in Fig. 3 and the increasing zero-crossing field difference for θ_K and ε_K in Fig. 4, if one considers the fact that both samples exhibit a different level of magneto-optical anisotropy (see Table 1), which leads to a crucial difference in how the transverse m_y magnetization contributes to θ_K and ε_K in either sample. This causes θ_K and ε_K not to vanish when $m_x = 0$ at a given applied field, and leads to a perceived coercive field shift in these MOKE measurements, depending on the level of magneto-optical anisotropy in the sample. Another significant feature is that this effect is not commensurate for Kerr rotation and ellipticity for complex τ values, as experimentally demonstrated in Figs. 3 and 4. We also confronted our measurements to the theory we developed above, by calculating the ΔH_0 vs. Φ_0 curves expected from the parameters in Table 1 and plotting them on top of the experimental data in Fig. 4. As can be observed, the agreement between theory and experiment is fully consistent, which confirms the complexity of magneto-optics we predicted upon existence of magneto-optical anisotropy, and for which the conventional MOKE geometry classification scheme breaks down. While a similar lack of correspondence between Kerr rotation and ellipticity has been observed in exchange-coupled magnetic multilayers [37,38], this behavior was attributed to optical interference effects. Instead, our study clearly demonstrates that this type of MOKE anomaly is caused by the presence of magneto-optical anisotropy. This is an issue of crucial relevance, as magneto-optical anisotropy can be produced by various agents such as epitaxial strain [29], surface patterning [35] or ultrathin noble metal overcoats, as in the present experiment, and is likely to be present in many samples that exhibit some level of anisotropy.

In conclusion, we studied both theoretically and experimentally how the lack of magneto-optical isotropy affects the MOKE signal, using the uniaxial magneto-optical anisotropy scenario as an example. We found that even for a purely in-plane oriented magnetization vector, the proportionality between the Kerr rotation or ellipticity and the

longitudinal component of magnetization does not generally persist in the presence of magneto-optical anisotropy. Instead, we discovered the existence of an anomalous magnetization dependence for the first-order magneto-optical Fresnel coefficients, and demonstrated its relevant impact on the accuracy of MOKE magnetometry measurements, if they are not properly interpreted. Our study reflects that caution is needed when collecting MOKE data in systems with low symmetry, since dissimilar magneto-optical coupling strengths along different orientations are bound to commonly exist in materials, even if their strength might not be as large as in our test samples, which we devised for the purpose of a clear experimental verification. Finally, we address the question of how magneto-optical Kerr effects should be classified, because the common dual definition based upon the Cartesian magnetization components **and** specific elements of reflection matrix cannot be maintained, given that this correspondence is only fulfilled for the special case of magneto-optical isotropy. Instead, we propose to redefine the longitudinal Kerr effect as the entirety of reflection matrix terms that are caused by the presence of a longitudinal component of magnetization, i.e. the magnetization component that is defined by the axis, in which the sample plane and the plane of incidence intersect. According to Eq. (5), this magnetization component m_x makes the conventional contribution to r_{sp} leading to Eq. (6), but also leads to a change in r_{pp} that is described by Eq. (5) if magneto-optical anisotropy is present. Correspondingly, the transverse MOKE effect describes the entirety of the reflection matrix terms caused by a transverse magnetization m_y. This transverse effect encompasses now not only the magnetic contribution to the p-polarization reflectivity term r_{pp}, but also the m_y dependent polarization change effect occurring in Eq. (6), which led to the experimental differences in between samples A and B due to their different magneto-optical anisotropy. Furthermore, we suggest correspondingly updated descriptions and definitions for the polar magneto-optical Kerr effect as including all effects caused by a polar magnetization component.

11

Footnotes

[footnote#1] We have chosen $e^{-i\omega t}$ as the time-dependent part of the solution for the wave equation, which yields $N = n + i\kappa$ and $Q = Q_r + iQ_i$ [24]. In the same way, the magneto-optical coupling factor is defined as $Q = -i\varepsilon_{xy}/\varepsilon_{xx}$, for $m_z = 1$. The sign of Q employed here agrees with the convention taken by Qiu and Bader [2], while it is the opposite of the one followed by You and Shin [23].

[footnote#2] We define r_p as the magnetization independent part of the reflection matrix element r_{pp}, in such a way that $r_{pp} = r_p + \beta m_y$. In magneto-optics, we can generally assume that $|\beta/r_p| \ll 1$.

[footnote#3] While sample-to-sample variations in the switching field, which results from a thermally activated process, are more common to exist even between samples with nominally identical magnetic properties, we focus here on the $m(H)$ trajectory sections governed by magnetization rotation, which are fully predictable upon knowledge of the anisotropy fields.

References

[1] M. J. Freiser, "A Survey of Magnetooptic Effects", *IEEE Trans. Magn.* **4**, 152 (1968)

[2] Z. Q. Qiu, and S. D. Bader, "Surface magneto-optic Kerr effect (SMOKE)", *J. Magn. Magn. Mater.* **200**, 664 (1999)

[3] E. R. Moog, S. D. Bader, "Smoke signals from ferromagnetic monolayers: p(1×1) Fe/Au(100)", *Superlattices Microstruct.* **1**, 543 (1985)

[4] C. Daboo, J. A. C. Bland, R. J. Hicken, A. J. R. Ives, M. J. Baird, and M. J. Walker, "Vectorial magnetometry with the magneto-optic Kerr effect applied to Co/Cu/Co trilayer structures", *Phys. Rev. B* **47**, 11852 (1993)

[5] A. Berger, and M. R. Pufall, "Generalized magneto-optical ellipsometry", *Appl. Phys. Lett.* **71**, 965 (1997)

[6] A. Berger, and M. R. Pufall, "Quantitative vector magnetometry using generalized magneto-optical ellipsometry", *J. Appl. Phys.* **85**, 4583 (1999)

[7] P. Vavassori, "Polarization modulation technique for magneto-optical quantitative vector magnetometry", *Appl. Phys. Lett.* **77**, 1605 (2000)

[8] H. F. Ding, S. Pütter, H. P. Oepen, and J. Kirschner, "Spin-reorientation transition in thin films studied by the component-resolved Kerr effect", *Phys. Rev. B* **63**, 134425 (2001)

[9] M. R. Pufall, C. Platt, and A. Berger, "Layer-resolved magnetometry of a magnetic bilayer using the magneto-optical Kerr effect with varying angle of incidence", *J. Appl. Phys.* **85**, 4818 (1999)

[10] J. Hamrle, J. Ferré, M. Nývlt, and Š. Višňovský, "In-depth resolution of the magneto-optical Kerr effect in ferromagnetic multilayers", *Phys. Rev. B* **66**, 224423 (2002)

[11] R. Morales, Z.-P. Li, O. Petracic, X. Batlle, I. K. Schuller, J. Olamit, and K. Liu, "Magnetization depth dependence in exchange biased thin films", *Appl. Phys. Lett.* **89**, 072504 (2006)

[12] J. McCord, "Progress in magnetic domain observation by advanced magneto-optical microscopy", *J. Phys. D: Appl. Phys.* **48**, 333001 (2015)

[13] D. A. Allwood, G. Xiong, M. D. Cooke, and R. P. Cowburn, "Magneto-optical Kerr effect analysis of magnetic nanostructures", *J. Phys. D: Appl. Phys.* **36**, 2175 (2003)

[14] E. Nikulina, O. Idigoras. P. Vavassori, A. Chuvilin, and A. Berger, "Magneto-optical magnetometry of individual 30 nm cobalt nanowires grown by electron beam induced deposition", *Appl. Phys. Lett.* **100**, 142401 (2012)

[15] E. Nikulina, O. Idigoras, J. M. Porro, P. Vavassori, A. Chuvilin, and A. Berger, "Origin and control of magnetic exchange coupling in between focused electron beam deposited cobalt nanostructures", *Appl. Phys. Lett.* **103**, 123112 (2013)

[16] M. Grimsditch, and P. Vavassori, "The diffracted magneto-optic Kerr effect: what does it tell you?", *J. Phys.: Condens. Matter* **16**, R275 (2004)

[17] E. Beaurepaire, J.-C. Merle, A. Daunois, and J.-Y. Bigot, "Ultrafast Spin Dynamics in Ferromagnetic Nickel". *Phys. Rev. Lett.* **76**, 4250 (1996)

[18] B. Koopmans, M. van Kampen, J. T. Kohlhepp, and W. J. M. de Jonge, "Ultrafast Magneto-Optics in Nickel: Magnetism or Optics?", *Phys. Rev. Lett.* **85**, 844 (2000)

[19] C. Fowley, *et al*., "Direct measurement of the magnetic anisotropy field in Mn–Ga and Mn–Co–Ga Heusler films" *J. Phys. D: Appl. Phys.* **48,** 164006 (2015)

[20] C. D. Stanciu, F. Hansteen, A. V. Kimel, A. Kirilyuk, A. Tsukamoto, A. Itoh, and Th. Rasing, "All-Optical Magnetic Recording with Circularly Polarized Light", *Phys. Rev. Lett.* **99**, 047601 (2007)

[21] C.-H. Lambert, *et al.*, "All-optical control of ferromagnetic thin films and nanostructures", *Science* **345**, 1337 (2015)

[22] G. Armelles, A. Cebollada, A. García-Martín, and M. U. González, "Magnetoplasmonics: Combining Magnetic and Plasmonic Functionalities", *Adv. Opt. Mater.* **1**, 10 (2013)

[23] C.-Y. You, and S.-C. Shin, "Generalized analytic formulae for magneto-optical Kerr effects", *J. Appl. Phys.* **84**, 541 (1998)

[24] R. Atkinson, and P. H. Lissberger, "Sign conventions in magneto-optical calculations and measurements", *Appl. Opt.* **31**, 6076 (1992)

[25] Š. Višňovský, "Magneto-optical permittivity tensor in crystals", *Czech. J. Phys. B* **36**, 1424 (1986)

[26] See supplementary material at {URL to be inserted by publisher}

[27] D. Weller, G. R. Harp, R. F. C. Farrow, A. Cebollada, and J. Sticht, "Orientation dependence of the polar Kerr effect in fcc and hcp Co", *Phys. Rev. Lett.* **72**, 2097 (1994)

[28] R. M. Osgood III, K. T. Riggs, A. E. Johnson, J. E. Mattson, C. H. Sowers, and S. D. Bader, "Magneto-optic constants of hcp and fcc Co films", *Phys. Rev. B* **56**, 2627 (1997)

[29] J. A. Arregi, J. B. González-Díaz, O. Idigoras, and A. Berger, "Strain-induced magneto-optical anisotropy in epitaxial hcp Co films", *Phys. Rev. B* **92**, 184405 (2015)

[30] P. Riego, *et al.*, to be submitted for publication (2016)

[31] D. Weller, and A. Carl, "Oscillatory Paramagnetic Magneto-Optical Kerr Effect in Ru Wedges on Co", *Phys. Rev. Lett.* **74**, 190 (1995)

[32] W. Yang, D. N. Lambeth, and D. E. Laughlin, "Unicrystal Co-alloy media on Si(110)", *J. Appl. Phys.* **85**, 4723 (1999)

[33] O. Idigoras, A. K. Suszka, P. Vavassori, B. Obry, B. Hillebrands, P. Landeros, and A. Berger, "Magnetization reversal of in-plane uniaxial Co films and its dependence on epitaxial alignment", *J. Appl. Phys.* **115**, 083912 (2014)

[34] J. A. Arregi, J. B. González-Díaz, E. Bergaretxe, O. Idigoras, T. Unsal, and A. Berger, "Study of generalized magneto-optical ellipsometry measurement reliability", *J. Appl. Phys.* **111**, 103912 (2012)

[35] J. A. Arregi, J. B. González-Díaz, N. Soriano, B. Mora, and A. Berger, "Surface-topography induced optical and magneto-optical anisotropy in permalloy gratings", *J. Phys. D: Appl. Phys.* **48**, 305002 (2015)

[36] K. Postava, D. Hrabovský, J. Pištora, A. R. Fert, Š. Višňovský, and T. Yamaguchi, "Anisotropy of quadratic magneto-optic effects in reflection", *J. Appl. Phys.* **91**, 7293 (2002)

[37] S.-K. Kim, J.-W. Lee, S.-C. Shin, and K. Y. Kim, "Contrasting hysteresis behaviors between the longitudinal magneto-optical Kerr rotation and ellipticity", *J. Appl. Phys.* **91**, 3099 (2002)

[38] Z. C. Zhao, H. Wang, S. Q. Xiao, Y. X. Xia, J. A. McGuire, Y. Ren, Q. Y. Jin, and T. R. Gao, "Anomalous hysteresis loops measured by the magneto-optical Kerr effect in a Co/NiO/Cu/Co/Cu structure", *J. Appl. Phys.* **101**, 016105 (2007)

Table 1

Sample	A (t_{Ru} = 0.3 nm)	B (t_{Ru} = 1.6 nm)
M_S (10^3 emu/cm^3)	1.17 ± 0.08	1.21 ± 0.09
H_{K1} (kOe)	1.28 ± 0.02	1.34 ± 0.03
H_{K2} (kOe)	2.02 ± 0.03	2.28 ± 0.05
$Re[Q_\parallel]$ (10^{-2})	2.7 ± 0.1	3.7 ± 0.2
$Im[Q_\parallel]$ (10^{-2})	-0.7 ± 0.1	0.2 ± 0.1
$Re[Q_\perp]$ (10^{-2})	2.849 ± 0.005	2.815 ± 0.008
$Im[Q_\perp]$ (10^{-2})	-2.133 ± 0.005	-1.981 ± 0.009
$Re[\tau]$	0.18 ± 0.03	-0.21 ± 0.05
$Im[\tau]$	-0.48 ± 0.05	-0.49 ± 0.03
$|\tau|$	0.52 ± 0.05	0.54 ± 0.03

Table 1. Experimentally determined magnetic anisotropy field and saturation magnetization parameters (top part) as well as magneto-optical parameters (bottom part). The error bars indicate the precision of all determined quantities.

Figure 1
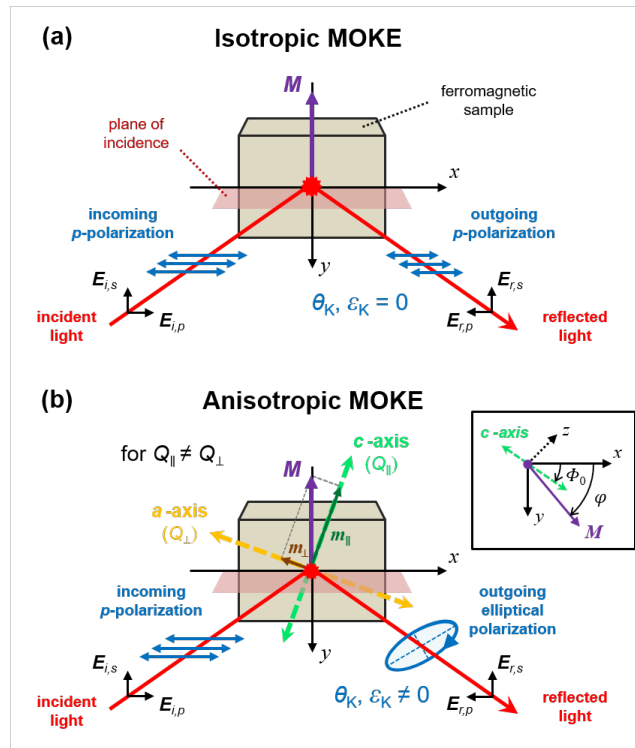
Fig. 1. Schematic of a MOKE experiment for isotropic vs. anisotropic first-order magneto-optics in the case of a *p*-polarized incident light and a transverse magnetization. The plane of incidence is contained in the xz plane. (a) In the case of isotropic magneto-optics, the outgoing polarization state is also purely *p*-polarized, from which null Kerr rotation and ellipticity follow. (b) On the contrary, the presence of uniaxial magneto-optical anisotropy causes an elliptically polarized reflected wave, resulting in non-zero Kerr rotation and ellipticity. The inset in (b) defines the deviation of the c-axis (Φ_0) and magnetization (φ) from the *x*-axis.

Figure 2
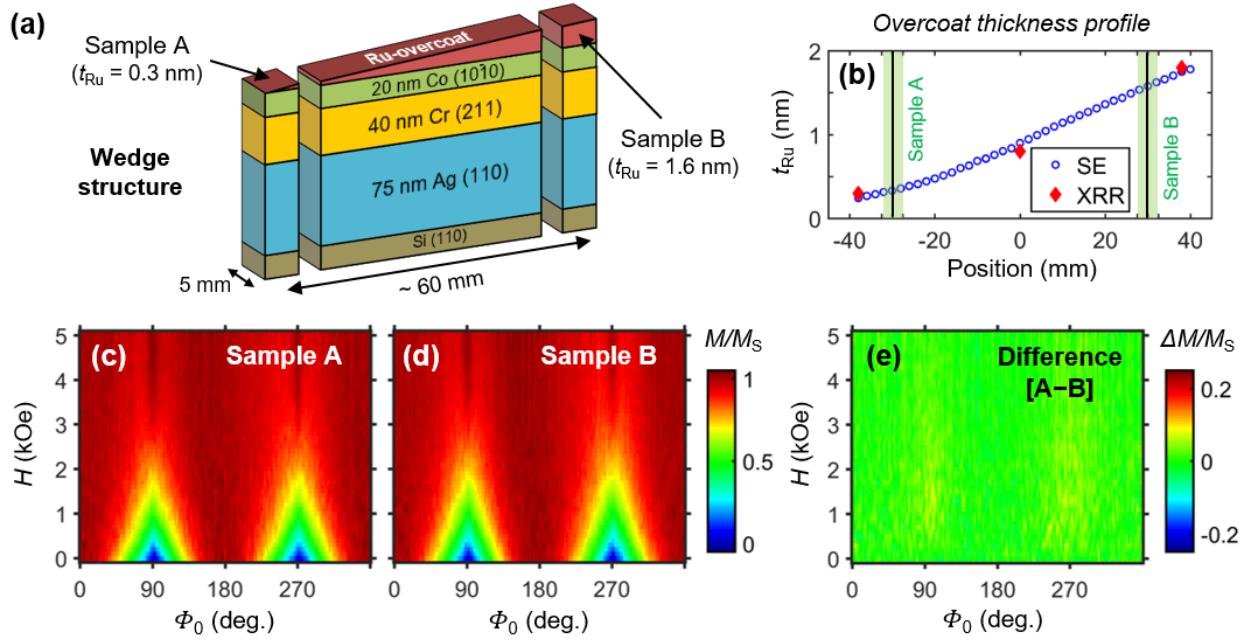
Fig. 2. (a) Schematic of the fabricated sample, consisting of a Ru-wedge deposited onto the Si(110)/Ag(110)/Cr(211)/Co(10$\underline{1}$0) epitaxial film sequence grown on an elongated wafer piece (~80 mm × 5 mm). The sample is covered by 10-nm-thick SiO$_2$ layer to avoid oxidation. Samples A and B are cut segments having Ru-thicknesses of 0.3 nm and 1.6 nm, respectively. (b) Ru-overcoat thickness profile as calibrated via spectroscopic ellipsometry (SE) and x-ray reflectivity (XRR). The shaded areas indicate the segments employed in this study as samples A and B. (c), (d) correspond to VSM measurements of samples A and B in the form of color-coded magnetization maps, displayed as a function of the applied field strength H and orientation Φ_0 with respect to the c-axis. (e) shows the difference of the magnetization maps in (c) and (d).

Figure 3
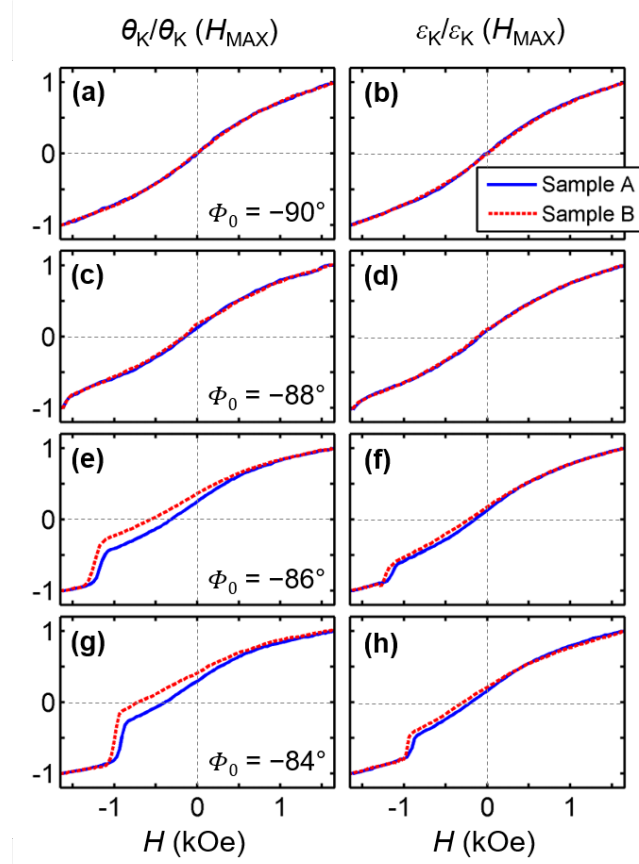
Fig. 3. Field-dependent magneto-optical measurements for Sample A (blue, solid line) and Sample B (red, dashed line) in terms of the Kerr rotation θ_K (left panel) and ellipticity ε_K (right panel) for c-axis orientations of (a)-(b) $\Phi_0 = -90°$, (c)-(d) $\Phi_0 = -88°$, (e)-(f) $\Phi_0 = -86°$ and (g)-(h) $\Phi_0 = -84°$. The data are scaled with respect to their values at $H = \pm 1.7$ kOe.

Figure 4
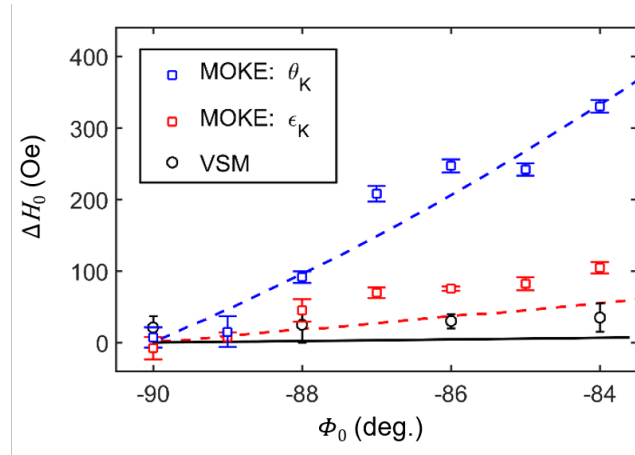
Fig. 4. Difference in zero-crossing field, $\Delta H_0 = H_0^B - H_0^A$ between Sample A and B vs. sample orientation Φ_0, as extracted from VSM, Kerr rotation θ_K and ellipticity ε_K. The dashed lines represent the theoretical predictions according to Eq. (6) and using the material parameters in Table 1. The solid black line is calculated by using the extracted magnetic anisotropy fields.